TRANSACTIONS OF THE INSTITUTE OF FLUID-FLOW MACHINERY

No. 126, 2014, 83–110

ANDRZEJ BŁASZCZYK*

Liquid flow parameters at the outlet of the formed suction intake with a rib

Technical University of Łódź, Institute of Turbomachinery, Wólczańska 219/223, 90-924 Łódź, Poland

Abstract

The article presents a procedure and the chosen results of numerical computations of liquid flow parameters, which use the data from their measurements realized on the test stand, for the model of formed suction intake with a rib, supplied by the screened open wet well. Comparative analysis of numerical computations and these determined by measurements, did concern the standard flow acceptance criteria.

1 Introduction

In water intakes of huge urban agglomerations as well as in cooling water condenser systems of the high power steam turbines there are the mixed flow and axial flow vertical pumps being applied. The water incoming to pumps in the neighborhood of intakes is to change the flow direction from horizontal to vertical. The change of the flow direction takes place in the inlet bells (Fig. 1a) or in formed suction intakes (Fig. 1b), which are the final elements of the intake channels of these pumps. Scheme of the real facility with marked intake channels, which final element is the formed suction intake shown in Fig. 2.

The real pumping station facility (Fig. 2) consists of: the screen chamber (1), where are the trash screens (2) used to roughly purify the water supply flowing in from the high-water source, (3) the rotary screen which task is to thorough purify the water from a pollution, (4) the open wet well, (5) the formed suction intake and (6) the place for the cooling water pump installation. In this scheme were marked the chosen geometrical parameters of the facility. Inlet bells Fig. 1a are used in pumps of the maximal efficiency $Q_{nom} = 15000$ m^3/h [10]. This kind of

*E-mail address: akblaszc@p.lodz.pl

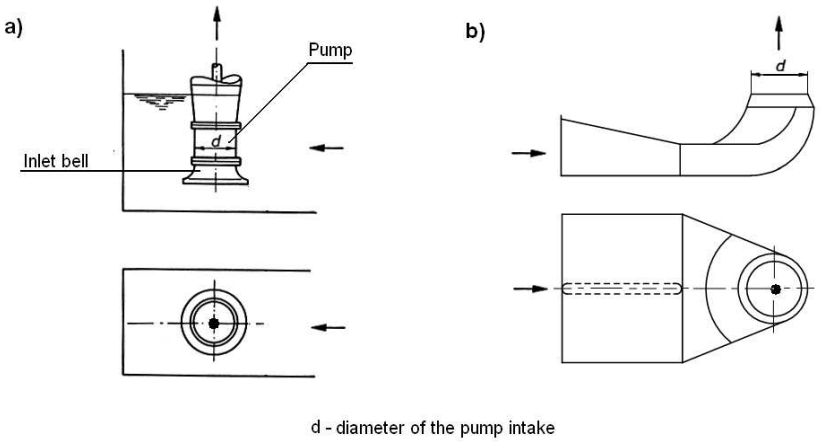

Figure 1. Suction intakes of pumps: a) inlet bell, b) formed suction intake.

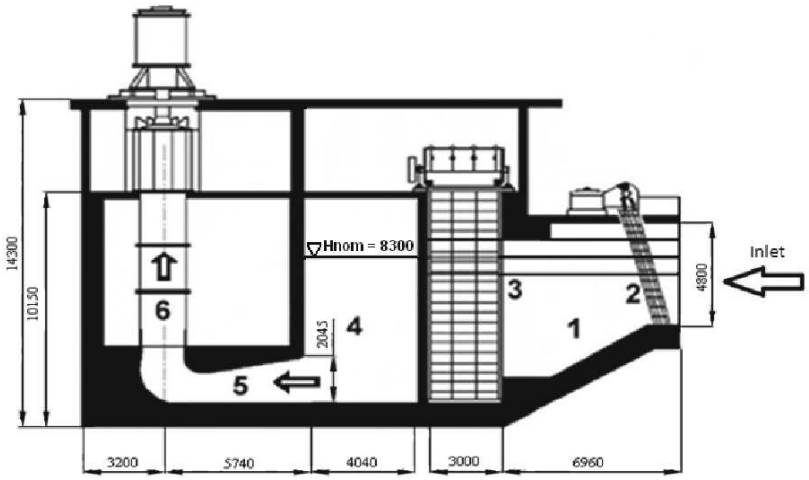

Figure 2. The real facility-system of intake channels [2,3].

intake is being used for a long time and constitutes the final element of the intake system for drawing the cooling water to the 200 MW units and less powerful.

Basic disadvantage of the inlet bell construction is:

- sensitiveness to various inflow conditions,
- non-uniform velocity profile before the impeller eye.

These defects have decided that in the case of pumps with capacities larger than $Q_{nom} = 15000$ m^3/h there are used formed suction inlets (Fig. 1b).

Design of the first type of formed suction inlets was to study the experimental models for future facilities. The geometrical scale of created model was varied and ranged from 1:10 to 1:20. Parameters of the flow channel were determined on the base of criterion numbers equalities for the model and the real facility.

Results of the multicriteria experimental studies have been used to develop recommendations ratio of geometrical parameters of the formed suction inlet compared in [1]. This ratio is shown in Fig. 4. In this standard are also given so called acceptance criteria relating to the flow parameters in the outlet of the formed suction inlet. However, there is lack of information in the available literature whether elaborated recommendations, based on the research, include the unsteady character of the flow in the suction inlet. Carried out research in the Turbomachinery Institute of Technical University of Łódź has revealed an occurrence of the unsteady hydraulic phenomena in the pump suction intakes.

2 Suction intake

Construction schemes of formed suction intakes were shown in Fig. 1 without the rib and with the rib in Fig. 4. In the paper there was introduced a flow through the formed suction intake with the rib to which the inflow is through the open wet well with a screen Fig. 11.

Geometry of the suction inlet has the major influence on formation of the liquid inflow to the pump. In the axial-flow and mixed flow pumps, in the case where the impeller eye is close to an outlet of the suction intake, the inflow velocity profile of a liquid to the impeller has the significant influence on the pump operation. In design of these pumps there is a uniform velocity profile taken into consideration, at the impeller eye. Due to this fact, the construction is required to preserve the velocity profile nonuniformity to be the least in relation to the average velocity in particular points of the intake cross-section.

The nonuniform velocity profile at the impeller eye may cause:

- decrease of the pump flow parameters H, Q – decreased capacity and head of the pump is caused by the axial flow symmetry unbalance, also resulting in the efficiency drop;
- formation of the transient whirls causing:
  1) additional dynamic loads at the impeller blades resulting in their decreased durability,
  2) change of the random flow parameters of the pump resulting in change of the operating point with the pump system (Fig. 3),
  3) vibration and noise of the pump.

Losses in the suction inlet have a direct influence on the hydraulic efficiency of the pump because they are counted for the total efficiency of the pump.

The following equation expresses the hydraulic efficiency of the pump:

$$\eta_h = \frac{H}{H + \Delta h_p} , \tag{1}$$

where: η_h – hydraulic efficiency of the pump, H – head of the pump, Δh_p – hydraulic losses in the pump in the neighborhood of flow from the suction to pumping elements.

In pumps with the high specific speed, which are the mixed flow and axial-flow pumps, losses in the suction inlet may cause the decrease of the total pump efficiency even over a dozen percent. In an poorly designed suction inlet may occur entry whirls, not taken into account during the design stage.This whirl may have the direction consistent with the direction of the impeller rotation and thus is called backward. A measure of the entry whirl is the absolute velocity circumferential component at the impeller eye c_{1u}.

In the case of the concurrent whirl there occur:

- decrease of the pump head (point B in Fig. 3) according to the equation

$$H = \frac{1}{g}(u_2 c_{2u} - u_1 c_{1u}) , \tag{2}$$

  because of the fact that in the axial-flow pumps $u_2 = u_1 = u$ the Eq. (2) adopts the form

$$H = \frac{1}{g} u (c_{2u} - c_{1u}) , \tag{3}$$

  where: H – head of the pump, g – acceleration due to the gravity, u_1 – circumferential velocity of the frame of reference at the intake of the impeller leading edge of the blade passage at the diameter D_1, u_2 – circumferential velocity of the frame of reference at the diameter of the trailing edge D_2, c_{2u} absolute velocity circumferential component of the medium at the impeller trailing edge, c_{1u} absolute velocity circumferential component at the impeller leading edge of the blade passage;
- efficiency loss;
- reduction of the power demand.

In the case of the backward whirl, there occur:

- increase of the head of the pump (point C in Fig. 3) according to equation

$$H = \frac{1}{g}(u_2 c_{2u} + u_1 c_{1u}) ; \tag{4}$$

- loss of the pump efficiency;
- increase of the power demand.

In Fig. 3 was shown the influence of the whirl on the flow parameters of the pumping system.

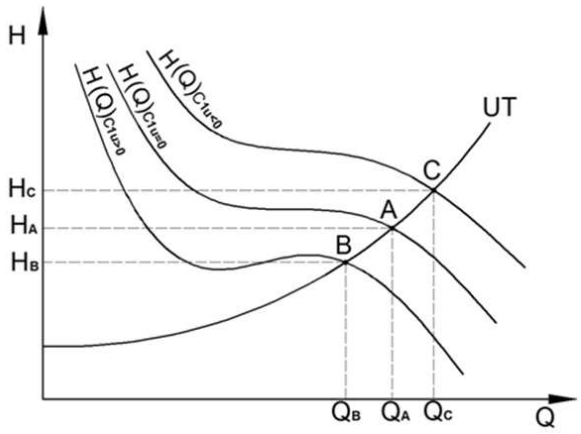

Figure 3. Flow characteristics of the pump and coordination points with the pumping system for different swirl cases [8].

In the case of the cooling water pumps, uncontrolled swirls may cause changes of the capacity (Fig. 3). Changes of the cooling water amount delivered to the turbine condenser may be the cause of the vacuum change in the condenser causing a power fluctuation in the power unit. Occurrence of the entry whirl not taken into account during the design step may cause an inflow of a medium to the impeller blades with a large angle of incidence causing the break of a stream. Break of a stream may cause the cavitation and increased hydraulic loss. This fact involves the load of bears of the rotating assembly, from very small to very large, fundamentally decreasing the durability of these pumps structural nodes. In order to reduce and even eliminate the enumerated hydraulic phenomena which randomly occur, there should be taken into account flow computation procedures of unsteady flows. At the moment, there is lack of publications concerning design methods of intakes of the formed suction intake type. At present, the most often design method of formed suction intakes is using the prescribed by the standard [1] dimensioning proposals introduced in the scheme, show in Fig. 4. In Fig. 4 all the geometric parameters refer to the pump inlet bell.

Standard [1] requires also that the flow in the suction inlet fulfill the following acceptance criteria:

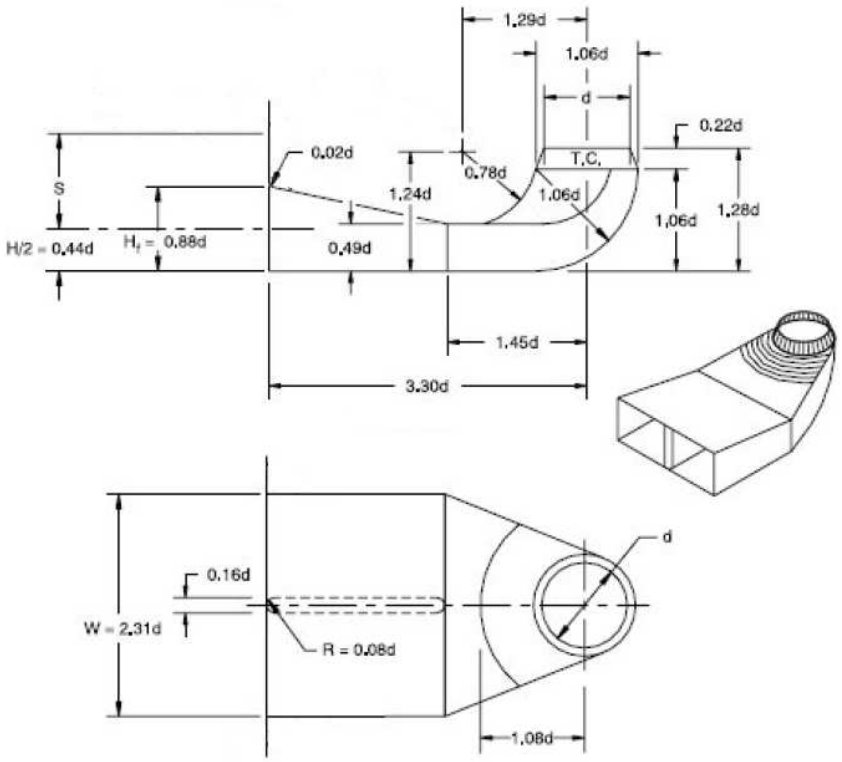

Figure 4. Characteristic dimensions of the formed suction intake recommended by [1].

- averaged in 10 min time the liquid angle of rotation in the pump intake cross-section $\Theta \leq 5^{o}$ – formula (18) (Fig. 15), it is allowed the momentary (to 30 sec.) deviation -$\Theta \approx 7^{o}$;

- nonuniformity of the velocity profile is less than 10% in every measurement point from the average value at the outlet pipe in the measurement cross-section;

- the velocity fluctuations in time in the given measurement point, using the probe, are less than 10% from the time averaged value this point.

Lack of the consistent design methods, in the past, resulted in the fact that for the same cooling water supply conditions of the cold end system of steam turbine, geometric parameters of the pump inlet channels fundamentally differed, not assuring the optimal pump operation conditions and were too expensive due to the large overall dimensions.

Comparison of the geometric parameters of the chosen suction inlet made

before introduction of the standard, in relation to recommended by [1] (Fig. 4) is put together in Tab. 1.

Table 1. Comparison of the geometric parameters of the chosen suction inlet made before introduction of the standard, in relation to recommended by [1].

Recommendations of norms	d	1.06d	1.06d	1.06d	1.06d	0.5d	0.22d	1.28d	1.29d	1.24d	0.49d	0.78d	3.3d	0.88d	2.31d
Dimensions given in [cm]															
Power plant 2															
Object	160	160	185	225.5	256.8	185.8	20	245.53	183.6	254.56	145.88	107.6	554.07	261	491
Norm	160	169.6	169.6	169.6	169.6	80	35.2	204.8	206.4	198.4	78.4	124.8	528	140.8	369.6
Difference	0	-9.6	15.4	55.9	87.2	105.8	-15.2	40.73	-22.8	56.16	67.48	-17.2	26.07	120.2	121.4
Percentage	0	5.66	9.08	32.96	51.42	132.25	43.18	19.89	11.05	28.31	86.07	13.78	4.94	85.37	32.85

Graphical illustration of the geometric parameters differences, compiled in Tab. 1, is shown in Fig. 5. It is to be noticed, that the manufactured formed suction intake is significantly bigger than recommended by the standard. Rib in the suction intake was constructed in its model after carrying out initial tests [2,3].

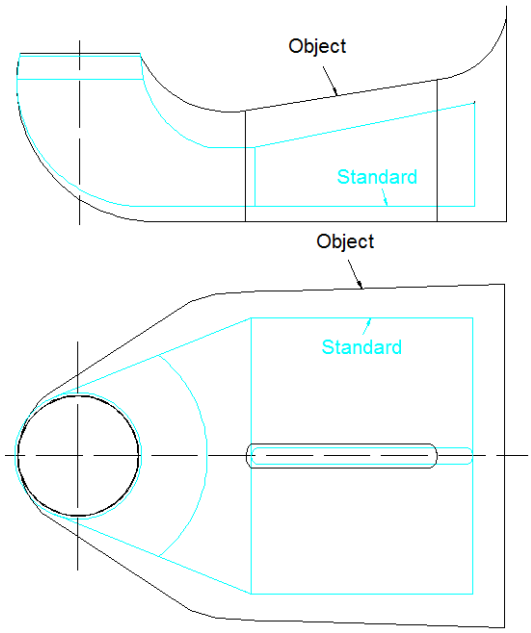

Figure 5. Comparison of the size of the suction intake made with and without the rib with recommended by the standard [1]

In the thesis [8] were included comparison results of other random objects. In all cases of constructed suction intakes were characterized by higher geometric parameters than recommended by the standard [1,2]. It should be stated that suction intakes recommended by the standard [1,2] sometimes do not fulfill the flow acceptance criteria imposed by the standard.

3 Numerical research of the unsteady flow in the suction intake with a rib

3.1 Introduction

Turbulent flow of the viscous, incompressible liquid is described by the Navier--Stokes equations, which along with the continuity equation constitute a complete dependence system allowing the determination of the pressure and flow velocity field. Time-averaged system was elaborated by Reynolds and constitutes the basic fluid mechanics formulas [6]. (N-S) equation takes the form:

$$\frac{\partial(\rho U_i)}{\partial t} + \frac{\partial(\rho U_j U_i)}{\partial x_j} = -\frac{\partial P}{\partial x_i} - \frac{\partial}{\partial x_j}\tau_{ij} + \rho g \ , \tag{5}$$

where: t –time, g – gravitional acceleration, U_j, U_i – momentary values of the velocity, P – momentary value of the pressure, x_i, x_j – geometric coordinates (Cartesian coordinate system), τ_{ij} – viscous stresses tensor.
Whereas the continuity equation takes the form

$$\frac{\partial U_i}{\partial x_i} = 0 \ , \tag{6}$$

$$U_i = \overline{U}_i + u_i \ , \tag{7}$$

where: U_i – momentary velocity value, $\overline{U}_i$ – average velocity value, u_i – value of the velocity fluctuation.
Graphical illustration of the Eq. (7) is shown in Fig. 6.

After taking into account that the momentary velocity can be described by the following dependence:

$$\overline{U}_i = \frac{1}{\Delta t} \int_t^{t+\Delta t} U_i \, dt \ , \tag{8}$$

there is obtained the time-averaged continuity using the Reynolds method (RANS) and the N-S equation for the incompressible fluid:

$$\frac{\partial \overline{U}_i}{\partial x_i} = 0 \ , \tag{9}$$

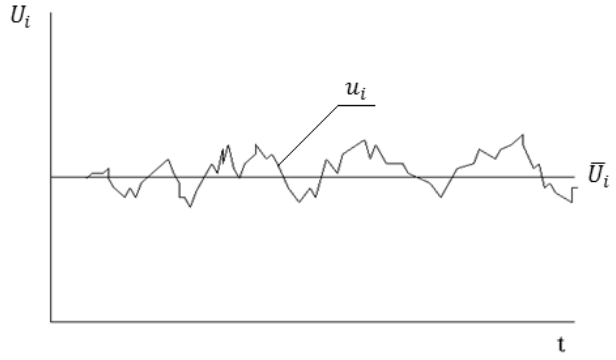

Figure 6. Momentary function of the velocity in time [13].

$$\underbrace{\frac{\partial(\rho\overline{U}_i)}{\partial t}}_{1}+\underbrace{\frac{\partial(\rho\overline{U}_j\overline{U}_i)}{\partial x_j}}_{2}=\underbrace{-\frac{\partial\overline{P}}{\partial x_i}}_{3}\underbrace{-\frac{\partial}{\partial x_j}(\overline{\tau}_{ij}+\rho\overline{u_iu_j})}_{4}+\underbrace{\rho g}_{5}\,, \tag{10}$$

where: (1) – time term, (2) – convection term, (3) – pressure term, (4) – diffusion term, (5) – mass forces term (taking into account the earthpull). Quantity $\overline{u_iu_j}$ is called the Reynolds stresses tensor and denoted as

$$\overline{\tau}_{ij}=-\rho\overline{u_iu_j}\,. \tag{11}$$

Stresses tensor requires modeling in order to close the (N-S) time-averaged equation using the turbulence model. For computations there was adopted the SST turbulence model.

3.2 Methodology and boundary conditions

Numerical computations of the flow have been carried out under the scheme elaborated by authors of the article shown in Fig. 7. Numerical computations under this scheme required the adoption of:

- the turbulence model,
- boundary conditions.

On the basis of assumptions from the comparative analysis and a result of the initial numerical computation made due to realization of the work [2,3], the SST turbulence model has been adopted.

The SST model proposed by Menter takes into account the transportation of the turbulent shear stresses in the turbulence model. In the SST model, the

adequate representation of the turbulent stresses transportation was obtained by using the limiter in formulation of the turbulent viscosity [13].

$$\mu_t = \frac{\rho a_1 k}{\max(a_1\omega, SF)} \,, \tag{12}$$

where: $a_1 0.31$ – coefficient, k – kinetic turbulence energy, ω – turbulence frequency, F – transition function, S – tensor invariant of the deformation velocity tensor.

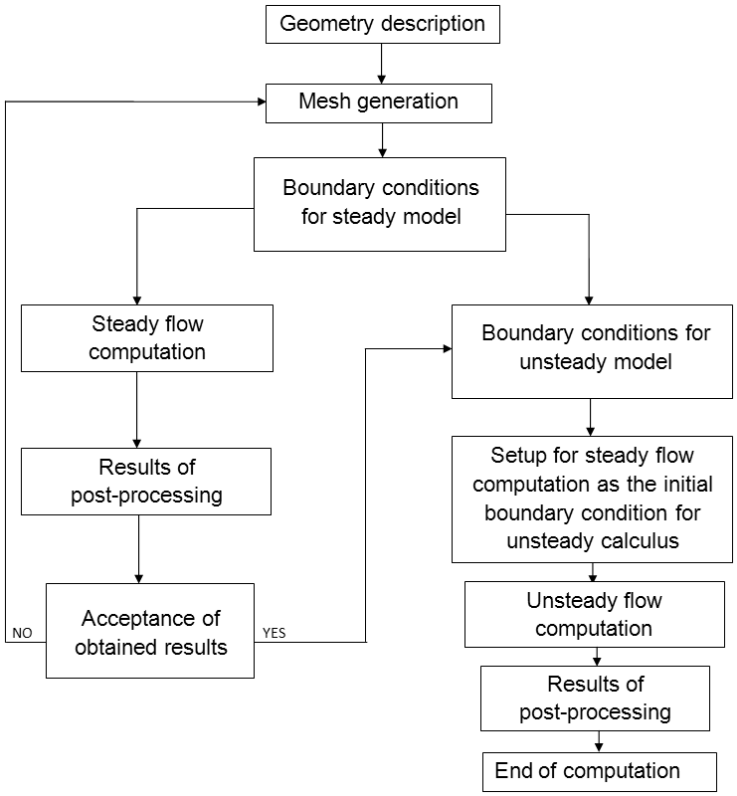

Figure 7. Scheme of the computation method of the unsteady flows in the suction intake.

In the adopted method, the transition function plays a major role. It is based on the distance value from the closest wall y and the flow parameters.

$$F = \tanh\left[\max\left(\frac{2\sqrt{k}}{\beta'\omega y'}, \frac{500\mu_t}{y^2\omega\rho}\right)\right]^2 \,, \tag{13}$$

where: k – kinetic turbulence energy, ω – turbulence frequency, μ_t – turbulence viscosity, y – value of the distance to the closest wall.

Numerical calculus under the scheme (Fig. 7) require the assumption of, common for steady and unsteady computations, boundary conditions:

- the total pressure in the inlet wet well defined by formula

$$p_c = \rho g H + \frac{\rho \left(\frac{Q}{A_l}\right)^2}{2} \tag{14}$$

  where: H – height of the water column in the wet well, ρ – water density, A_l – surface area of the connector of the screen chamber and the inlet of the wet well, Q – volume flow rate;

- a condition for the free surface generation according to the Fig. 8;

- the turbulence intensity at the level of 5 % (when $I = 10$) according to a formula:

$$I = \frac{\mu_t}{\mu_d}\,, \tag{15}$$

  where: μ_t – turbulent viscosity, μ_d – dynamic viscosity;

- mass flow of the outflow pipe: $\dot{m} = 24.6$ kg/s;

- the zero gradient of the pressure in the direction of the main flow (this condition is assumed internally by the preprocessor).

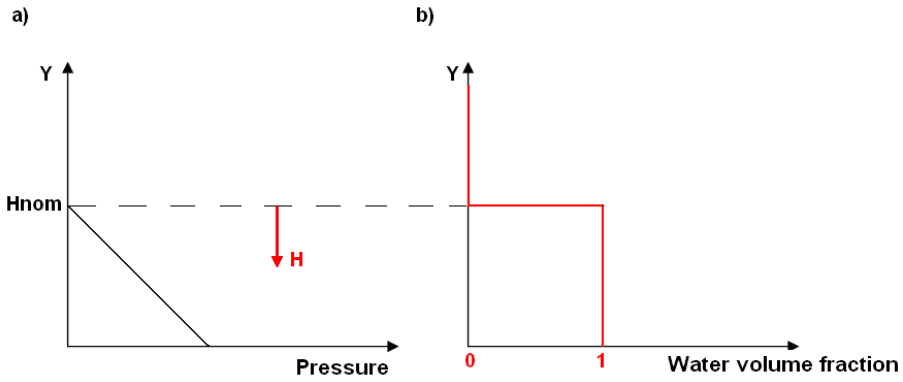

Figure 8. Boundary conditions of the inlet in the computational area of the inlet chamber: a) hydrostatic pressure b) water volume fraction.

Unsteady conditions require additional settings.

- work area of the rotary screen to the total area of the screen is 74%

- assumed loss of pressure at the screen $\Delta p = 60$ Pa,
- quadratic resistance coefficient:

$$K_Q = \left(\frac{\Delta p}{\Delta x}\right) {c_{por}}^2 \,, \tag{16}$$

where: Δp – pressure loss at the porous surface, Δx – thickness of the screen (porous surface), c_{por} – flow velocity of the liquid through the porous surface;

- hydraulically smooth walls have been assumed;
- a logarithmic velocity distribution on the wall has been assumed – the so-called wall function. In Fig. 9 below has been shown the diagram of dimensionless velocity u^+ in the function of dimensionless distance from the wall y^+. To have the wall function working correctly, the first mesh node has to lie in the distance not smaller than $y^+ = 12$ and not further than $y^+ = 200$ (Fig. 10). For the value $y^+ < 11$ the mesh node lies in the laminar sub-layer and for $y^+ > 300$, beyond the boundary layer.

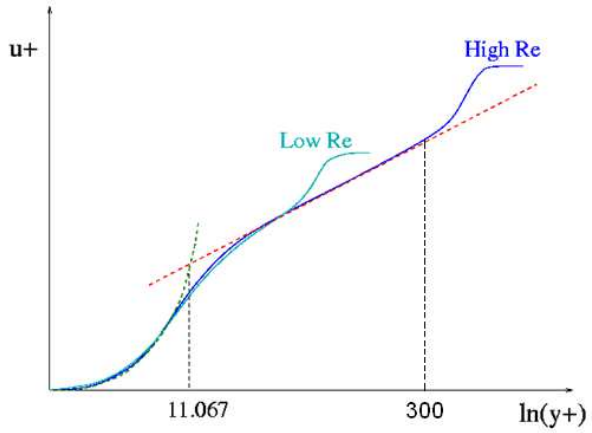

Figure 9. The range of values y^+ [14].

- Courant number – is the basic criterion of the unsteady flow calculus defined as

$$\text{Courant} = \frac{\text{u}\Delta\text{t}}{\Delta\text{x}} \,, \tag{17}$$

where: u – the average velocity, Δt – the time step, Δx – the size of the mesh cell.

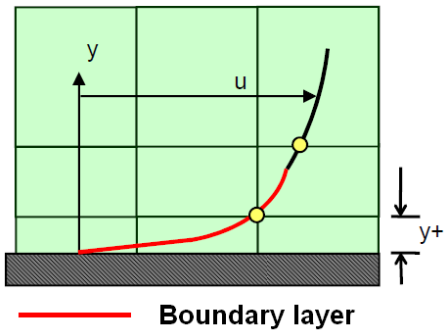

Figure 10. The position of the first mesh node in the boundary layer in the area of logarithmic velocity distribution (boundary layer) [14].

The scope of Courant number values, for the numerical computations, using the turbulence model SST, is not formulated. It is advisable to take such value, which allows for obtaining solution with the assumed level of convergence [14]. In considered models of the wet well and the formed suction intake, the value of Courant number is ranged in the scope (0.08–2.04) and for this value there was obtained the assumed level of convergence:

- the total time of computations: 30 s,
- the time step: 0.001 s,
- the minimal number of iterations for the given time step: 1,
- the maximal number of iterations for the given time step: 12,
- the degree of discretization of the convection term with the discretization coefficient 0.75 (0 – discretization of the first order, 1 – discretization of the second order),
- the discretization of the convection term: approximation of the second order derivatives backward (second order backward Euler),
- the solution recording time step: 0.05 s,
- tetrahedral mesh used in numerical computations,
- amount of control volumes in the case of the intake with barriers equals to $\approx 2.4 \times 10^6$, without barriers equals to $\approx 1.6 \times 10^6$,
- number of the mesh nodes for the intake with and without barriers equals to $\approx 1 \times 10^6$.

Geometry and the computation mesh is shown in Fig. 11.

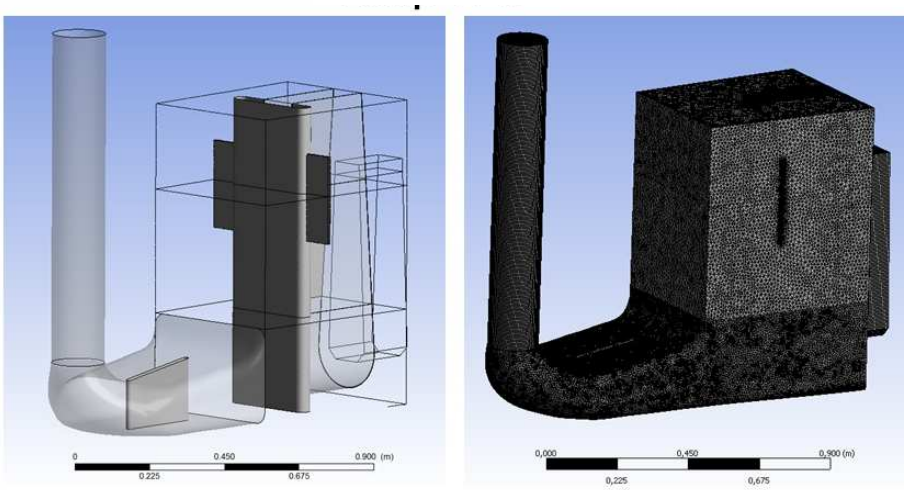

Figure 11. Geometry and computation mesh for the model of the intake with barriers.

The analysis of obtained results of the unsteady computations quality consisted of checking the level of unbalanced mass flows and momentum in the control volumes of the mesh – a so called residuum [14] (it determines the quality of obtained results), which for the each of the results was in the range of 10^{-4}–10^{-5}. This level informs that the solution has a good convergence and which results will be validated with observations taking place on the test stand.

3.3 Numerical calculus plan of the unsteady flow

Numerical computations of the unsteady flow in a model of the suction intake were realized for $(Q_{nom})_m = 88.702$ m^3/h, $(H_{nom})_m = 0.665$ m, which were corresponding with the intake nominal operation conditions in the facility $(Q_{nom})_o =$ 28050 m^3/h), $(H_{nom})_o = 8.3$ m. Scheme of the intake model with the rib is shown in Fig. 12. Numerical computations of the unsteady flow were carried out for the nominal level of the liquid in the open wet well ($H_{nom} = 8.3$ m Fig. 2) and nominal pump capacity ($Q_{nom} = 28050$ m^3/h). In researches of the model at the test stand these values were corresponding with values $H_{nom} = 0.665$ m, $Q_{nom} = 88.702$ m^3/h. Results of numerical computations were verified by results of computations using measurements on the test stand.

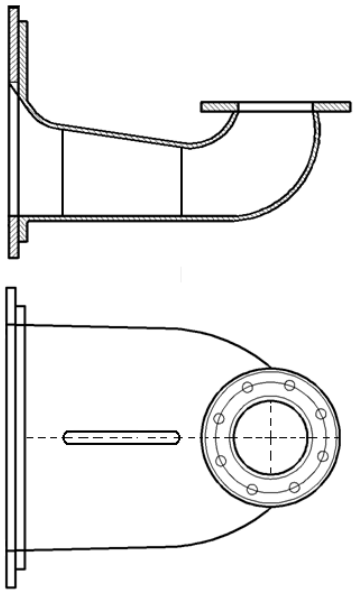

Figure 12. Model of the formed suction intake with the rib.

4 The test stand

4.1 Construction of the stand

The test stand enabled carrying out measurements and observations of the flow in the model in 1:10 scale shown in Fig. 13. Geometrical and flow parameters of the model were determined on the basis of the Froude (Fr) numbers equality condition for the facility and the model $\mathrm{Fr}_o = 1.094 \approx \mathrm{Fr}_m = 1.093$. Because the Reynolds' number $\mathrm{Re} > 3 \times 10^4$ and the Weber number $\mathrm{We} > 120$, far outweigh the critical values, it can be stated that the dynamic similarity condition between the object and the model is satisfied [1].

The test stand is shown in Fig. 13 consists of: the screen chamber (1), inlet screens (2), the rotary screen (3), the wet well (4), the formed suction intake (5), the swirl meter (6), the Pitot probe (7), pipelines (8), the flowmeter (9), the steam-water separation tank (10), the circulating pump (11), the main water tank (12), the delivery channel – model of the high-water source (13).

The view of the apparatus shown in Fig. 14. Measurement of the rotation angle Θ consisted in counting full rotations made by a swirl meter in the period of 30 s. From a side of the flow, rotations clockwise were treated as negative. For the angular velocity of the swirl meter, n, the average angle of the liquid rotation

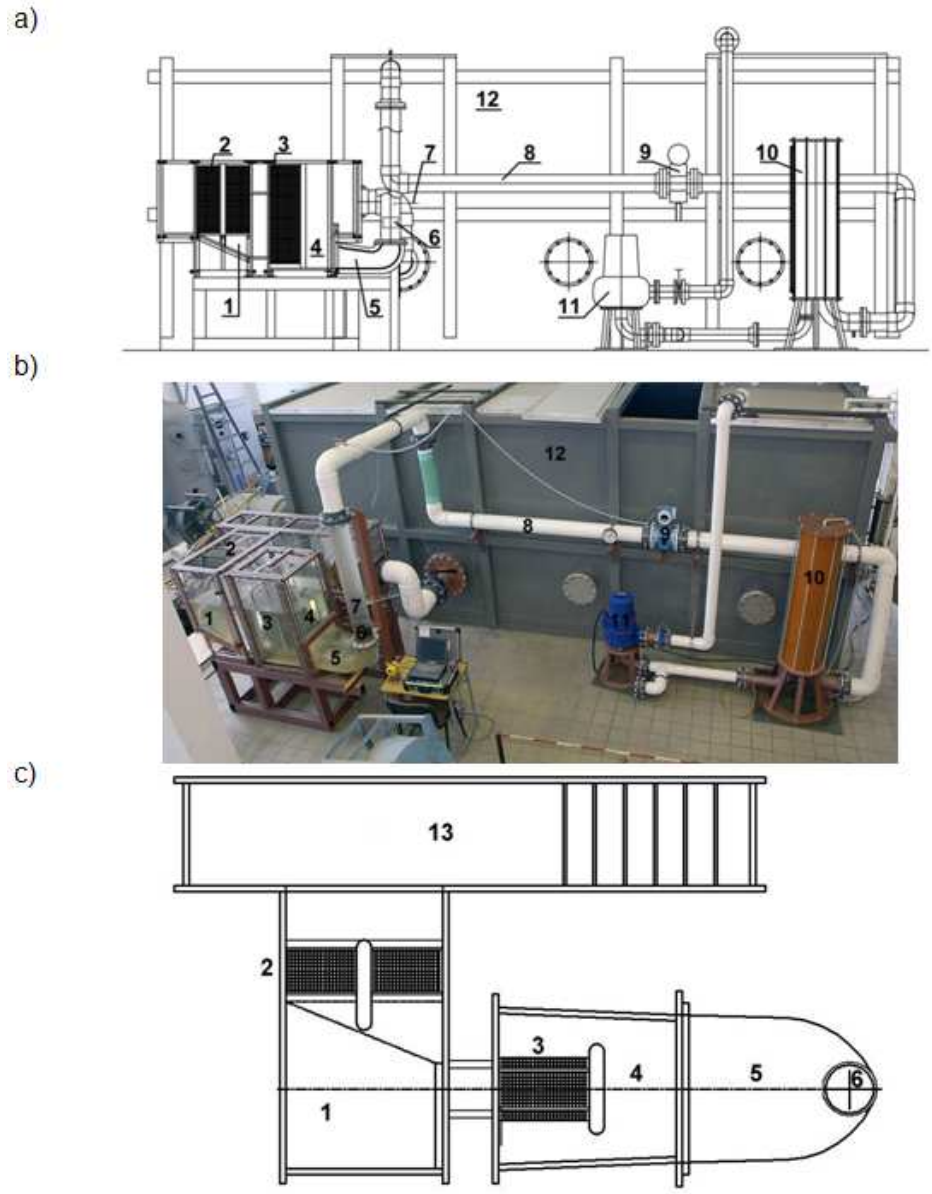

Figure 13. The test stand [2,3]: a) elevation of the test stand, b) view of the test stand, c) system of the wet well (top view).

in accordance to the Fig. 10, following equation determines:

$$\Theta = \tan^{-1} \frac{\pi D_m n}{c_a} \,. \tag{18}$$

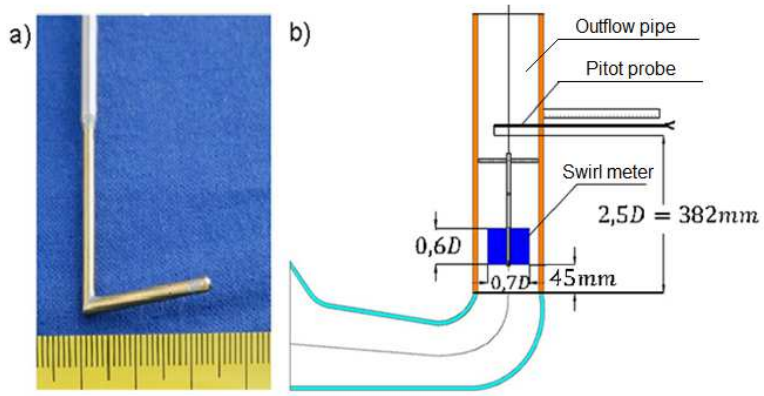

Figure 14. The built-up scheme of the Pitot probe and a swirl meter in the outflow pipe: a) view of the probe, b) swirl meter.

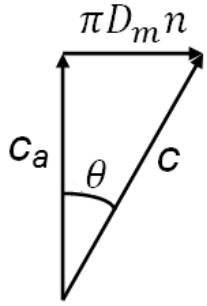

Figure 15. Velocity triangle in the zone of the swirl meter.

Value c_a of the average axial velocity at the measurement segment of the outflow pipe is a result of quotient of the capacity Q (measured using the electromagnetic transducer PROMAG 53WDN150 with exacitude of 0.2% of Endress+Hauser company) and the surface area of the pipe of $D_m = 153$ mm. diameter.

Liquid velocities and their changes in time in consecutive points of measurements (Fig. 14) were measured using the Pitot probe after constructing it into the outflow pipe. Diameter of the tip of the Pitot probe was 3 mm. View of the tip of the probe is shown in Fig. 18. Signals from the probe were transmitted to the differential transducer of the Mobrey company type 4301D2 with the set-up measurement from -2500 up to +2500 Pa. View of the apparatus for carrying out the measurements is shown in Fig. 16.
The measurement system enabled to record the 2048 samples in the time of 128 seconds using the Pitot probe. Calibration characteristic curve is shown in Fig. 17.

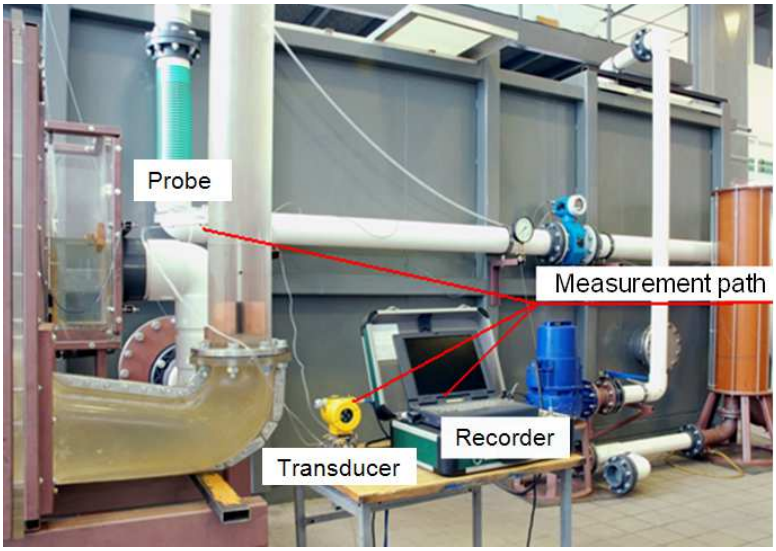

Figure 16. The measurement apparatus set for the Pitot probe.

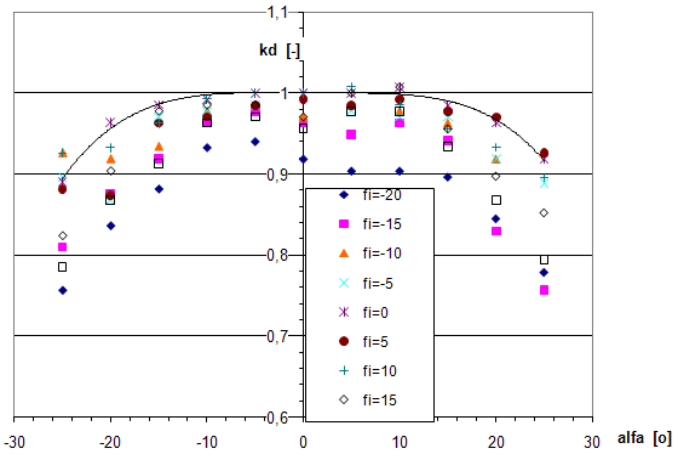

Figure 17. Directional characteristic of the Pitot probe.

Radii determining the location of the measurement points are described by dependences:

$$R_0 = 0 \cdot R = 0 \,, \tag{19}$$

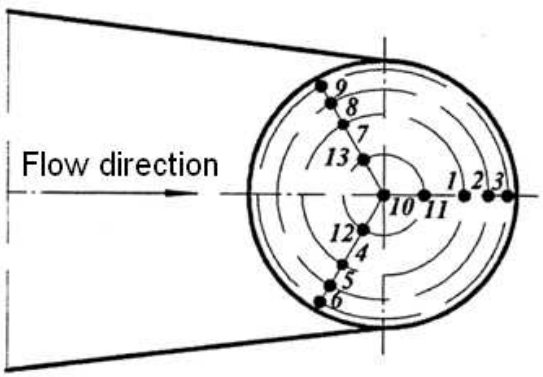

Figure 18. Measurement points of the Pitot probe in the outflow pipe.

$$R_1 = \frac{\sqrt{\frac{1}{5}} + \sqrt{\frac{2}{5}}}{2} R = 0.5398 \times 7605 = 41.3 \text{ mm}, \tag{20}$$

$$R_2 = \frac{\sqrt{\frac{2}{5}} + \sqrt{\frac{3}{5}}}{2} R = 0.7035 \times 7605 = 53.8 \text{ mm}, \tag{21}$$

$$R_3 = \frac{\sqrt{\frac{3}{5}} + \sqrt{\frac{4}{5}}}{2} R = 0.8345 \times 7605 = 41.3 \text{ mm}, \tag{22}$$

$$R_4 = \frac{\sqrt{\frac{4}{5}} + 1}{2} R = 0,9472 \times 7605 = 41.3 \text{ mm}. \tag{23}$$

5 Numerical computations versus velocity measurements comparative analysis

A subject for measurements were:

- angle of rotation of the liquid Θ in the cross-sectional area of the suction intake (inlet to the pump) Fig. 15,
- velocities in the plane of the Pitot probe measurement (outlet from the outflow pipe Fig. 14.

5.1 Angle of rotation of the liquid

For determination of the angle of rotation of the liquid there have been used numerical computation results of the flow in the zone of a swirl meter in time and values determined basing on the measurements realized on the test stand (Fig. 13). In [8] it is said, that the direct influence on the angle of rotation of the liquid, have the circumferential components c_u.

5.1.1 Numerical computations of the circumferential component $\mathbf{c_u}$

Numerical computations of velocities were carried out according to the algorithm explained in Section 3 in nineteen control surfaces. These surfaces were away from each other in a distance of 5 mm along the swirl meter height, which limit location in relation to the outlet of the suction intake was shown in Fig. 19.

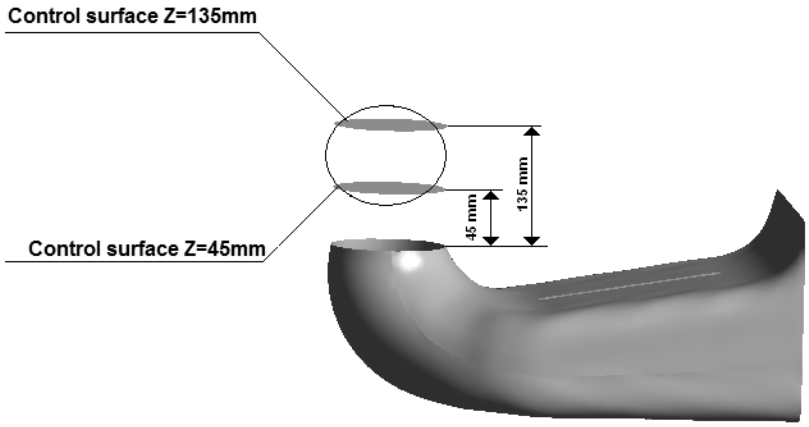

Figure 19. Computational surfaces of the flow in the zone of the swirl meter.

Computations were realized for the nominal operation parameters of the suction intake $(H_{nom})_m$ $(Q_{nom})_m$ and the liquid flow time of 30 seconds. Adopted time of measurements of 30 s was corresponding to the time of counting rotations of the swirl meter n Eq. (18) for determination of the angle Θ of a single point in the graph (Fig. 22b). Total measurement time of the swirl meter rotation on the test stand was 30 min.

Numerical computations of the circumferential component c_u in the function of time, shown in Fig. 20. In this figure there was shown the course of the function in 30 s time of the averaged value c_u in the whole swirl meter area. Value of that velocity was determined as the arithmetic average of the velocity c_u, averaged in nineteen control surfaces. In this graph there was also marked the level of average velocity c_u. Points a and b are the marked maximum and minimum values

of the circumferential component c_u, which are equal correspondingly $(c_u)_a = -0.0295$ [m/s] and $(c_u)_b = -0.0140$ [m/s]. Values c_u shown in Fig. 20 were used in Eq. (18) in order to compute the angle Θ.

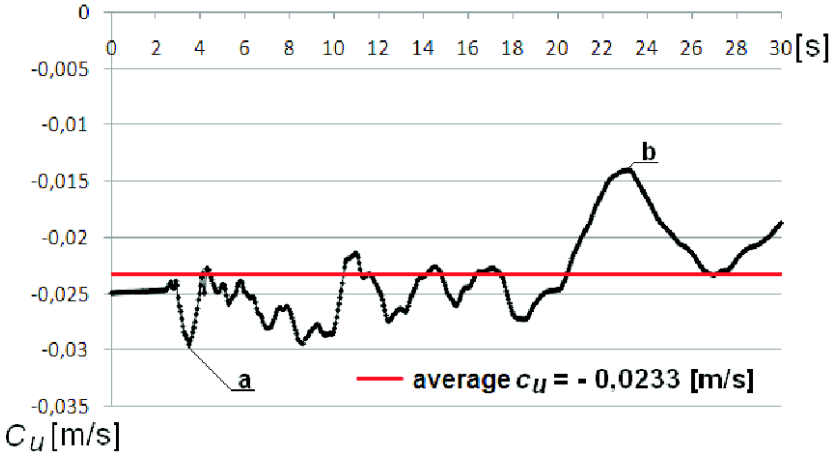

Figure 20. Numerically computed momentary values of the circumferential velocity component in the whole swirl meter zone.

5.1.2 Determinations of the swirl angle Θ on the basis of measurement results

Measurements of rotation velocities of the swirl meter n for computations of the angle Θ were carried out for nominal operation conditions of the suction intake $(H_{nom})_m$ and $(Q_{nom})_m$. Main and construction dimensions of the outflow pipe are shown in Fig. 14. Total time of the measurement was 30 min. Number of rotations of the swirl meter was registered every 30 s. There were counted only full number of rotations made by a swirl meter. Results of measurements and computations of the angle Θ were placed in [2,3]. Graphical illustration of results of measurements was shown in Fig. 22b.

5.1.3 Comparative analysis of measurements and computations results of the liquid swirl angle Θ

In computations of the swirl angle Θ there were used:

- averaged values of the velocity circumferential component c_u in a time function (Fig. 20),
- averaged value of the velocity axial component c_a, as is shown in Fig. 21,

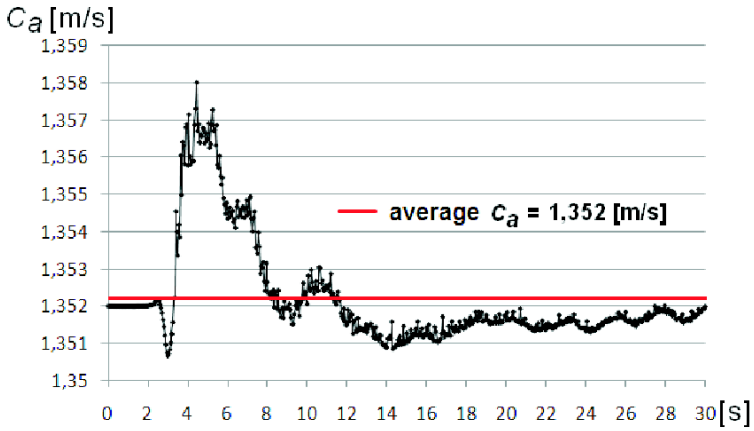

Figure 21. Numerically computed momentary values of the velocity axial component in the whole zone of the swirl meter.

- results of measurements of the circumferential velocity of the swirl meter on the test stand.

Values of the swirl angle Θ on the basis of numerical computations results were determined by the formula

$$\Theta = \tan^{-1} \frac{c_u}{c_a} \,. \tag{24}$$

Value of the angle Θ based on measurements results were determined by Eq. (18).

Results of measurements in a form of graphs were shown in Fig. 22a and drawing 22b. As agreed in Section 4.1, shown in Fig. 22b location of measurement points given in the Section 4.1, shown in Fig. 22b location of measurement points takes into consideration a direction of the swirl meter rotations. In these graphs there were found averaged values of the angle Θ. In the evaluation of the minimum and maximum amplitudes, there were used absolute values of the angle. In the graph 22a there were marked by point 'a' the maximum $\Theta_a = -1.25$, by point 'b' minimum $\Theta_b = -0.6^{\circ}$ amplitude of the angle Θ.

In the graph 22b the maximum value of the angle in 'Point 1' is equal $\Theta = 6.5^{\circ}$, minimum value of the angle $\Theta = -0.68^{\circ}$ is characterizing 27 measurements points which constitutes closely 50% of all the points. In the graph 22a, a single value of the time is corresponded by a single value of the swirl angle Θ. However, in the graph 22b, a single value of the time is corresponded by one or two values of the swirl angle Θ. Two values of the swirl angle Θ occur in a case while the swirl meter is during observations of 30 s period, and was rotating alternately in two directions. Because of this, it should be noticed that a change of the swirl direction was marked in [2,3] using the opposed sign. And because of that, in Fig. 22b there occur minus values of the angle Θ. In the graph 23 there was shown

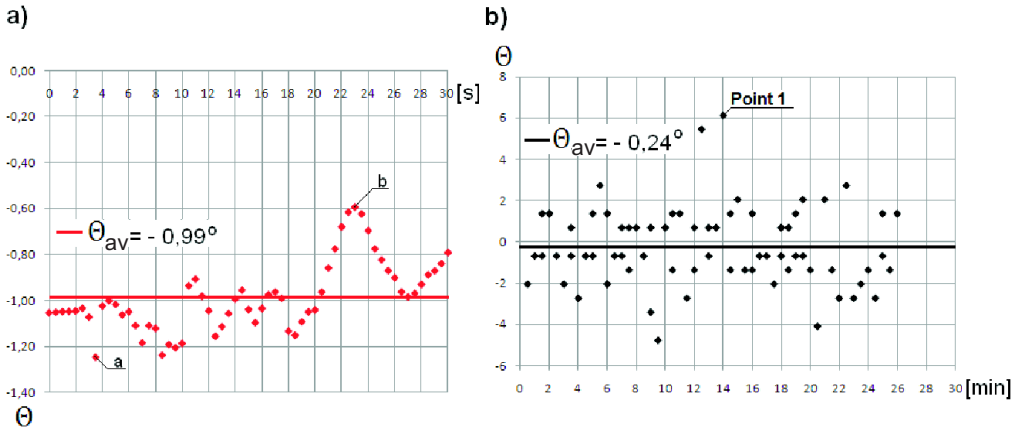

Figure 22. Change of the swirl angle in a function of time: a) $\Theta(t)$ on the basis of measurement results; b) set of points obtained on the basis of the number of rotations measurements of the swirl meter in a time of 30 min.

a graph illustrating changes of the swirl angle in the period of 30 s obtained on the basis of numerical computations results. In this figure, there were also marked the levels of minimum values of the angle Θ (27 points) and values of average angles from numerical computations and measurements results.

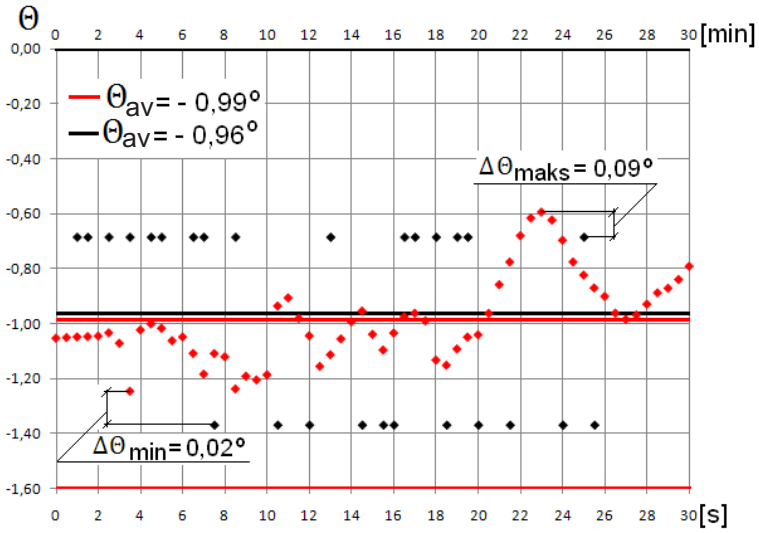

Figure 23. Course of the function of variety of the angle Θ in the period of 30 s on the basis of numerical computations. Black color points are the marked levels of minimum values of the angle Θ computed on the basis of measurements.

From the graph in Fig. 18, there are known:

- average values of the angle Θ from numerical computations and computations on the basis of measurements, differ by $\Delta\Theta_{average} = -0.03^{o}$,
- difference between the maximum amplitudes is $\Delta\Theta_{max} = 0.09^{o}$,
- difference between minimum amplitudes is equal to $\Delta\Theta_{min} = 0.02^{o}$.

5.2 Velocities in the plane of the Pitot probe measurements

Results of numerical computations of velocities and measurements of the time function in the Pitot probe measurement points were shown in the graph in Figs. 24a and 24b. In these graphs there were marked with a broken line, the value of average velocity in the Pitot probe measurement cross-section, while using the dotted line, the scope of velocity fluctuations.
By comparison of the velocity changes computed numerically, Fig. 24a, on the basis of measurements Fig. 24b, it follows that:

- Any of the measurement points of the probe, meet the acceptance citerion which applies to 10% of a scope of accepted velocity fluctuations;
- Course of the velocity change measured at points 2, 3, 4, 5, 7, and 8 is placed over the average, while at points 9, and 10 is under,
- Curves of the graph 24a obtained on the basis of the measurement, stay under the value of the average velocity.

Averaged velocity values obtained from numerical computations and measurements using the probe, were shown in Fig. 25. In the graph there were also marked values of average velocities from numerical computations and measurements and allowable by the standard [1] 10% of fluctuations of the profile. Value of the average velocity at point 10, is out of the average velocity value of velocities in other points. The probable cause of underevaluation at the point 10, is a measurement in a zone of a trace of the swirl meter axis. By giving up the average value in the point 10, there has been obtained a new location of the average velocity value of all the measurement points (Fig. 26).

6 Conclusions

Based on the observations given in Sections 5.1.1 and 5.2.2, it can be stated that the proposed unsteady flow measurement method is suitable use in the supply conditions analysis for mixed and axial-flow pumps of vertical axis. This method will allow for the better understanding of the flow structure in pump suction intakes and will limit the costs of model examinations.

Received 15 October 2014

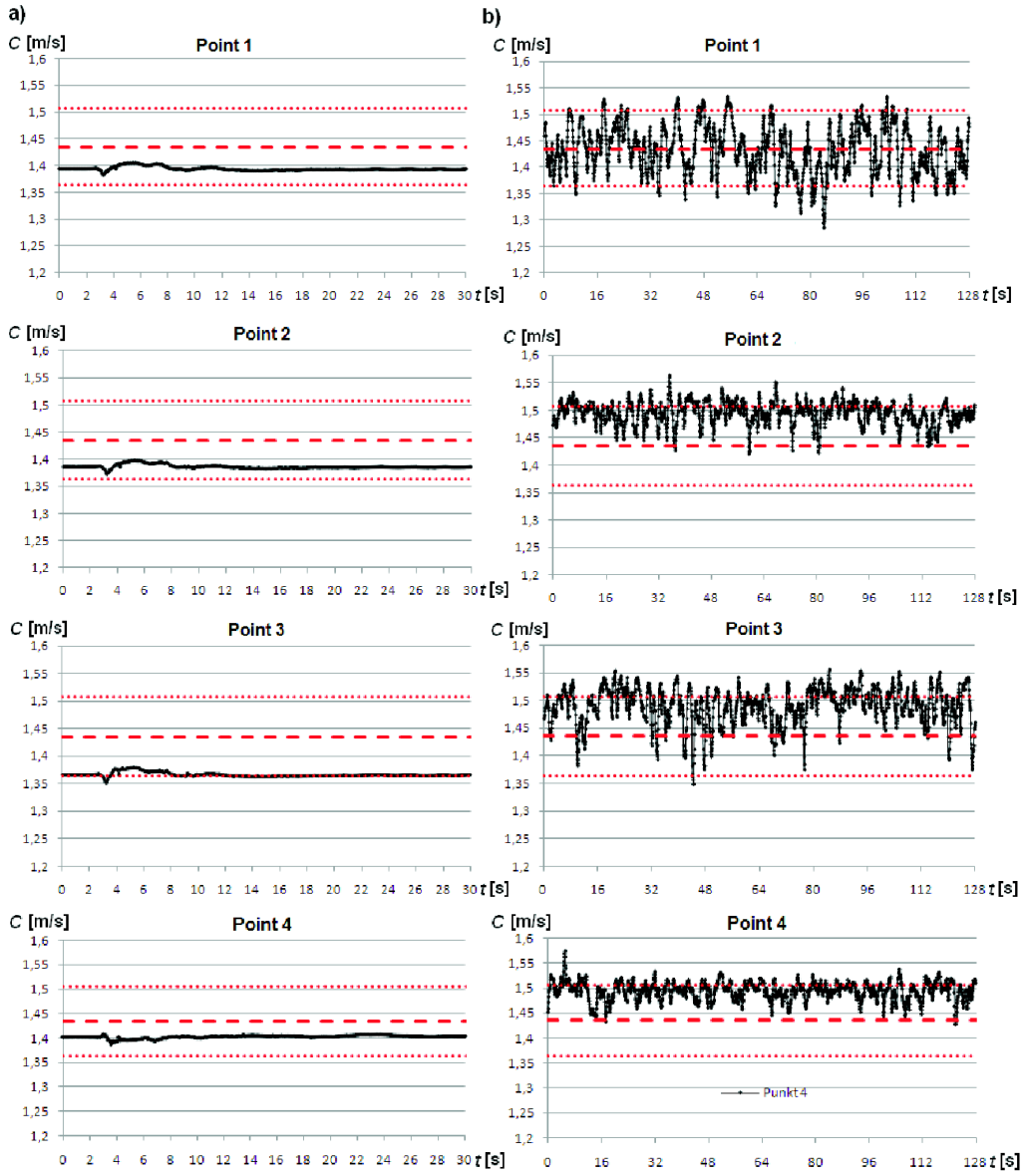

Figure 24. For caption see page 109.

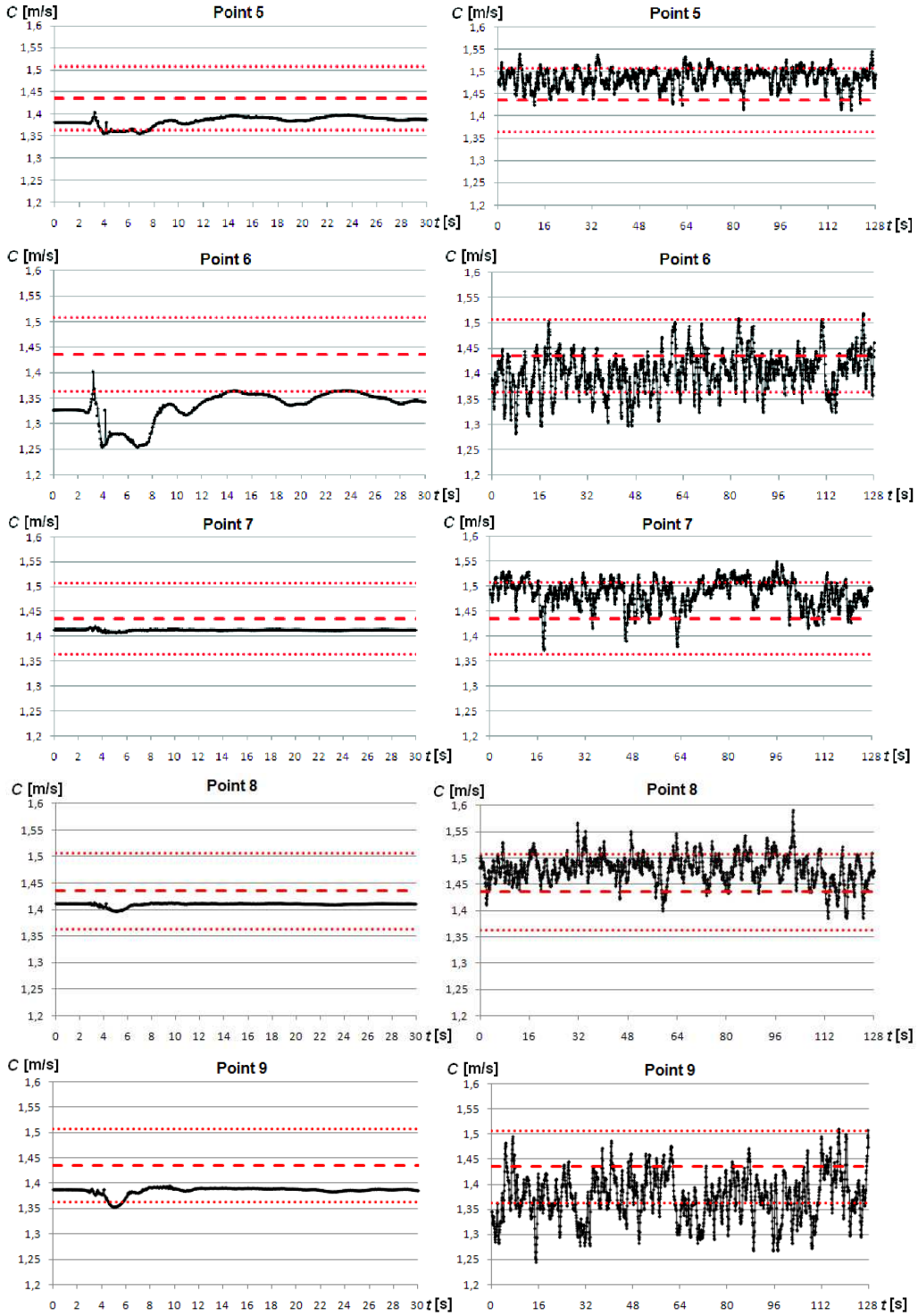
C [m/s]
Point 5
t [s]
C [m/s]
Point 5
t [s]
C [m/s]
Point 6
t [s]
C [m/s]
Point 6
t [s]
C [m/s]
Point 7
t [s]
C [m/s]
Point 7
t [s]
C [m/s]
Point 8
t [s]
C [m/s]
Point 8
t [s]
C [m/s]
Point 9
t [s]
C [m/s]
Point 9
t [s]

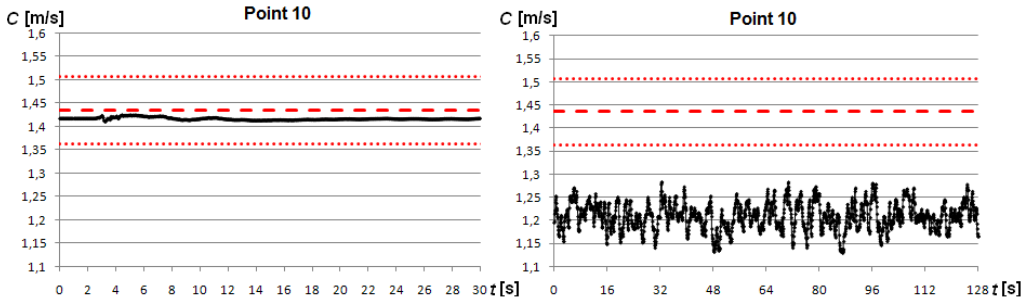

Figure 24. Changes of the velocity in points of the Pitot probe measurements in a function of time: a) according to numerical computations, b) from the Pitot probe measurements.

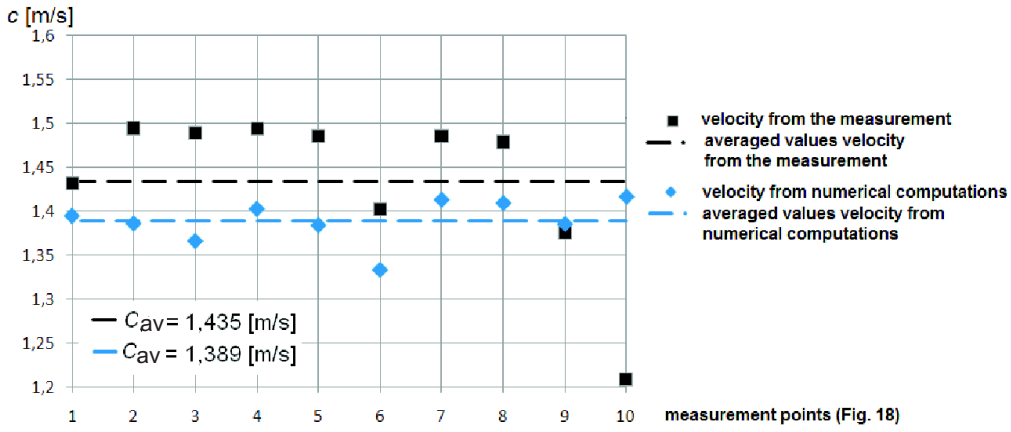

Figure 25. Averaged values of the velocity in points of measurements and from numerical computations.

References

[1] American National Standard for Pump Intake Design. ANSI/HI 9.8-1998. Hydraulic Institute. 9 Sylvan Way, Parsippany, New Jersey 07054-3802, www.pumps.org

[2] Błaszczyk A., Głuch J., Gardzilewicz A.: *Operating and econimic condition of cooling water control for marine steam turbine condensers.* Polish Maritime Res. (2011), 3, 48–54.

[3] Błaszczyk A., Najdecki S., Papierski A., Staniszewski J.: *Model examinations of the suction intake of the cooling water pump 180P19 on the test stand no. 8 for a unit A 460 MW in Pątnów Power Plant.* Report of I stage works, Arch. IMP PŁ 1542, Łódź 2006.

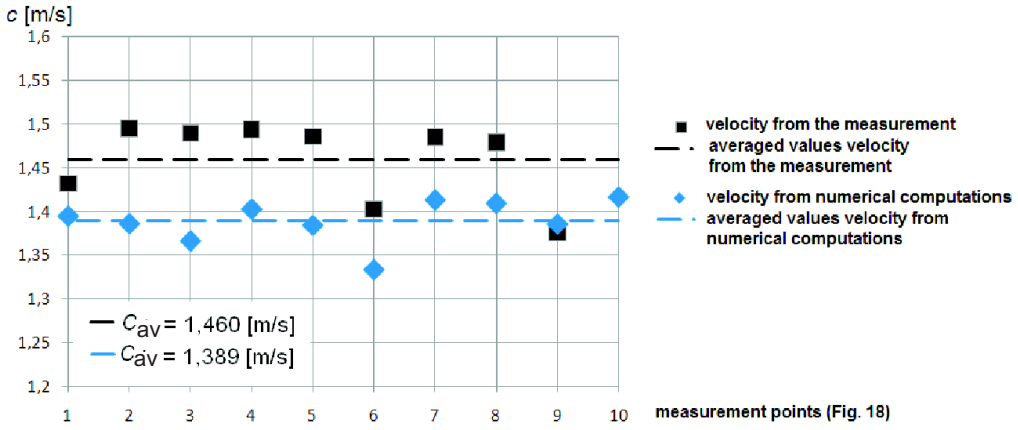

Figure 26. Averaged velocity values at points of measurements and computed numerically.

[4] Błaszczyk A., Najdecki S., Papierski A., Staniszewski J.: *Model examinations of the suction intake of the cooling water pump 180P19 on the test stand no. 8 for a unit A 460 MW in Pątnów Power Plant.* Report of II stage works, Arch. IMP PŁ 1546, Łódź 2006.

[5] Błaszczyk A., Susik M.: *Concept for a flow structure investigations in pump wet wells, taking into consderation steady flows.* Turbomachinery **137**(2010), 23–32, Lodz University of Technology, Institute of Turbomachinery.

[6] Kazimierski Z.: *Fundamentals of fluid mechanics and flow simulation computer methods.* Lodz University of Technology, Łódź 2004 (in Polish).

[7] Kunicki R.: *Numerical and experimental investigations of unsteady flows in pump wet wells.* PhD thesis, Lodz University of Technology, Łódź 2011.

[8] Stępniewski M.: *Pumps.* WNT, Warsaw 1985 (in Polish).

[9] Zaino A.: *Influence of construction parameters on flow conditions in closed wet wells of huge centrifugal pumps.* Wrocław University of Technology, Wrocław 1994.